JVST B
Journal of Vacuum Science & Technology B

ARTICLE

avs.scitation.org/journal/jvb

Temperature dependence of the infrared dielectric function and the direct bandgap of InSb from 80 to 725 K

Cite as: J. Vac. Sci. Technol. B **41**, 022203 (2023); doi: 10.1116/6.0002326
Submitted: 2 November 2022 · Accepted: 13 January 2023 ·
Published Online: 13 February 2023

Melissa Rivero Arias, Carlos A. Armenta, Carola Emminger,[a] Cesy M. Zamarripa, Nuwanjula S. Samarasingha, Jaden R. Love, Sonam Yadav, and Stefan Zollner[b]

AFFILIATIONS

Department of Physics, MSC 3D, New Mexico State University, P. O. Box 30001, Las Cruces, New Mexico 88003-8001

Note: This paper is a part of the Special Topic Collection Honoring Dr. Gary McGuire's Research and Leadership as the Editor of the Journal of Vacuum Science & Technology for Three Decades.

[a] **Present address:** Felix-Bloch Institut für Festkörperphysik, Universität Leipzig, Linnéstraße 5, 04103 Leipzig, Germany, and Institut für Physik, Humboldt-Universität zu Berlin, Zum Großen Windkanal 2, 12489 Berlin, Germany.
[b] **Electronic mail:** zollner@nmsu.edu

ABSTRACT

The temperature dependence of the complex pseudodielectric function of bulk InSb (100) near the direct band gap was measured with Fourier-transform infrared ellipsometry between 30 and 500 meV at temperatures from 80 to 725 K in ultrahigh vacuum. Using the Jellison–Sales method for transparent glasses, the thickness of the native oxide was found to be 25 ± 5 Å, assuming a high-frequency dielectric constant of about 3.8 for the native oxide. After this surface correction, the dielectric function was fitted with a Herzinger–Johs parametric semiconductor model to determine the bandgap and with a Drude term to determine the electron concentration and the mobility. We find that the bandgap decreases from 230 meV at 80 K to 185 meV at 300 K, as expected from thermal expansion and a Bose–Einstein model for electron-phonon scattering renormalization of the bandgap. Between 450 and 550 K, the bandgap remains constant near 150 meV and then increases again at even higher temperatures, presumably due to a Burstein–Moss shift resulting from thermally excited electron-hole pairs. The broadening of the direct bandgap increases steadily with temperature. The electron concentration (calculated from the Drude tail at low energies assuming parabolic bands with a constant electron mass of $0.014m_0$) increases from 2×10^{16} cm^{-3} at 300 K to 3×10^{17} cm^{-3} at 700 K, in reasonable agreement with temperature-dependent Hall measurements. The electron mobility was found to decrease from 10^5 cm^2/Vs at 450 K to 2×10^4 cm^2/Vs at 700 K, also in good agreement with Hall effect results. We describe a theoretical model that might be used to explain these experimental results.

Published under an exclusive license by the AVS. https://doi.org/10.1116/6.0002326

I. INTRODUCTION

Indium antimonide (InSb) is a III–V compound semiconductor with the zinc blende crystal structure.[1–3] Of all III–V semiconductors, it has the smallest bandgap[4,5] (only 185 meV at 300 K) and, therefore, the smallest electron mass[4] ($0.014m_0$) and the strongest nonparabolicity effects.[1,6] It also has the largest spin-orbit splittings[1,4] and the smallest optical phonon energies.[7] The valence band maximum and the conduction band minimum are at the Γ-point of the Brillouin zone. The satellite valleys in the conduction band are at least 500 meV above the Γ-minimum and do not need to be considered for the interpretation of our experiments.[8,9]

The properties of InSb, especially the intrinsic carrier concentration,[3,10–15] the band structure,[8,16] and band filling, due to doping[17–19] (Burstein–Moss shift) were studied extensively from the 1950s to the 1980s. It was noted that InSb was the only elemental or III–V semiconductor where degenerate carrier statistics with Fermi–Dirac distribution functions had to be considered.[20] For most other semiconductors with larger bandgaps, such as Ge or GaAs, nondegenerate (Maxwell–Boltzmann) statistics can be

Published under an exclusive license by the AVS

applied, which has led to the textbook theories of intrinsic semiconductors.[21,22] The absorption coefficient and the refractive index near the direct bandgap were determined using transmission and interference measurements[23–25] and from spectroscopic ellipsometry.[26] It is difficult to determine the absorption coefficient from transmission measurements alone, because the reflection losses depend on the refractive index, which may not be known with sufficient precision to calculate the absorption coefficient from the transmittance. This difficulty can be overcome by measuring the transmission of several samples with different thicknesses.[27,28]

Temperature-dependent ellipsometry measurements of InSb were performed in the region of interband transitions (above the direct bandgap) by Logothetidis *et al.*[29] as well as by others.[30] The infrared dielectric function of InSb near the direct bandgap was measured by Schaefer *et al.*[26] and explained with a theoretical model. There are several experimental reports and calculations[9,31,32] of the temperature dependence of the direct bandgap up to room temperature[13] using transmission measurements,[28,33] photoluminescence,[34,35] piezoreflectance,[36] and two-photon Hall response.[37] The only data available above room temperature seem to be the transmission data by Liu and Maan,[28] which, unfortunately, are not compatible with our ellipsometry results at the highest temperatures. While transmission measurements determine small absorption coefficients ($20-300\,\mathrm{cm}^{-1}$) of the Urbach tail below the band gap, ellipsometry is more sensitive to large absorption coefficients $>1000\,\mathrm{cm}^{-1}$ near and above the bandgap.

Open questions to be addressed by our work are the following: (1) How does the direct bandgap vary with temperature between room temperature and the melting point at 800 K? (2) How does the intrinsic carrier concentration depend on temperature?[15] and (3) How does this affect the optical absorption?[38] (4) What is the role of excitons in optical absorption?[39] and (5) How do excitons get screened[40,41] above 300 K due to thermally excited electron-hole pairs? (6) What is the temperature dependence of the electron[42] and hole[15] effective masses?[43] (7) Are the effective masses determined by the unrenormalized bandgap (including thermal expansion) or by the renormalized bandgap due to deformation-potential electron phonon interaction?[15,43,44] (8) Does InSb become a semimetal (a semiconductor with zero bandgap) or a topological insulator at high temperatures?[31] (9) How do the longitudinal optical phonons couple to the thermally excited carriers?[28]

Our findings are relevant not only for InSb, but also for all small-gap semiconductors considered for mid-wave infrared detectors, such as $\mathrm{Ge}_{1-y}\mathrm{Sn}_y$ alloys.

II. EXPERIMENT AND DATA ANALYSIS

The pseudodielectric function in the region of the direct bandgap of a commercially obtained undoped bulk InSb sample with (100) surface orientation was measured between 80 and 725 K using a J. A. Woollam Fourier-transform infrared variable angle spectroscopic ellipsometer (FTIR-VASE) equipped with a Lakeshore ST-400 ultrahigh vacuum (UHV) cryostat and diamond windows as described elsewhere.[45] As received, the back surface of the sample was rough and we did not attempt to roughen it further. Reflections from the back surface led to depolarization effects and artifacts in the data at the longest wavelengths, especially at low temperatures, as described below. The sample was cooled with liquid nitrogen and heated with a resistor. The temperature was measured with two type-E (NiCr-CuNi) thermocouples, one attached to the sample (more accurate) and the other located near the heater (more stable control). Our InSb substrate melted at a thermocouple reading of 750 K, lower than the melting point of InSb (800 K).[46] It is, therefore, likely that the sample temperature (above 300 K) is somewhat higher than the reading of the thermocouple attached to the sample. This temperature difference is smaller at room temperature and increases to about 50 K near the InSb melting point.

The FTIR-VASE resolution was set to $16\,\mathrm{cm}^{-1}$ (2 meV), which is smaller than the E_0 broadening at the lowest temperatures (4 meV, as shown below). Room temperature data in air were also taken from 0.5 to 6.5 eV on a J. A. Woollam VASE ellipsometer for comparison with the literature.[29,47] All measurements were performed at 70° angle of incidence.

Before the measurements, the InSb sample was cleaned ultrasonically, first in water for 15 min and then in isopropanol for 15 min. We did not use the harsh chemicals (bromine solution in methanol, hydrochloric acid diluted with methanol) as suggested by Aspnes and Studna.[47] The pseudodielectric function of InSb measured at room temperature in air from 0.5 to 6.5 eV before and after this wet clean is shown in Fig. S1.[61] By comparison with the optical constants of Ref. 47 for InSb (especially the maximum of $\langle\epsilon_2\rangle$ at the E_2 critical point near 3.7 eV) and Refs. 48 and 49 for its native oxide, the surface layer thickness in air was found to be 36 Å before cleaning and 29 Å after wet cleaning.

After the wet clean, the InSb sample was mounted in the UHV cryostat, which was then pumped down to a base pressure below 10^{-8} Torr.[45] We tried several methods of mounting the sample.[45] Our best results were obtained by clamping the sample to the copper sample holder with stainless steel strips and screws, without the use of any adhesives, silver paint, etc. The sample was then heated at 450 °C for more than 12 h to remove volatile surface layers such as water (known as a degas) and allowed to cool back down to room temperature. The pseudodielectric function of InSb at 300 K was then acquired on the FTIR-VASE instrument inside the cryostat under UHV conditions. Window corrections[45] were applied automatically by our commercial data acquisition software.

To correct the pseudodielectric function and obtain an estimate for the dielectric function of InSb, the thickness and optical constants of the oxide must be known. We assume a constant value of $\epsilon_\infty = 3.8$ for the native oxide on InSb in the infrared spectral region.[48] Since the oxide thickness is small, the errors introduced by lattice absorption of oxygen-related vibrational modes in the native oxide will be small.

To determine the oxide thickness, we use the Jellison-Sales method for transparent glasses,[50] which is based on the premise that the imaginary part of the dielectric function for an insulator must be exactly zero in the transparent region below the bandgap (not positive, not negative). If one assumes an oxide thickness that is too small, the resulting dielectric function of InSb will be positive. If the oxide thickness is assumed too large, then the corrected dielectric function will be negative. Using this premise, we were able to determine that the thickness of the native oxide is 25 ± 5 Å. The accuracy of this method is determined by the

Published under an exclusive license by the AVS

systematic and statistical errors of the ellipsometric angle Δ in the transparent region, including the window correction, which affects the ellipsometric angle Δ. This method does not work for conductors (such as InSb at high temperatures) since the free carrier absorption obscures the transparent region below the bandgap. See Fig. S3 in the supplementary material for more information.[61]

After this sample preparation, the InSb substrate was cooled down to 80 K and FTIR-VASE spectra were taken up to 750 K in steps of approximately 25 K. The resulting pseudodielectric functions are shown in Fig. S4 in the supplementary material.[61] Important trends can already be observed in these $\langle\epsilon\rangle$ spectra, as described in the supplementary material.[61] At the lowest temperatures, there are incoherent reflections from the back side of the sample (and the sample holder), which lead to artifacts in the pseudodielectric function and strong depolarization effects below 0.1 eV. At higher temperatures, the transmission of the substrate decreases due to free carrier absorption and the artifacts at long wavelengths disappear.

Our previous studies on GaP[51] and Ge[52] showed that the oxide thickness can vary by 20–30 Å when performing a temperature series. We ignore these variations for this work because small fluctuations in the oxide thickness do not have a significant impact on the temperature dependence of the bandgap, which is the primary focus of our work. There is no indication in the pseudoabsorption below the bandgap that oxide thickness variations with temperature were significant.

The dielectric function ϵ, calculated from $\langle\epsilon\rangle$ assuming a constant oxide thickness of 25 Å, is shown in Fig. 1. We observe a number of trends: (1) The E_0 bandgap, seen as the onset of absorption and as a peak of ϵ_1, decreases from the lowest temperatures (purple) to room temperature (blue), remains constant near 500 K (yellow), and then increases again at the highest temperatures (red). (2) The broadening increases monotonically with temperature. (3) Above room temperature, ϵ_1 diverges toward $-\infty$ at the lowest photon energies, while ϵ_2 diverges towards $+\infty$. This indicates free carrier absorption, consistent with a Drude model, at elevated temperatures. (4) There is a 30% decrease in the magnitude of ϵ_2 at high energies (near 0.5 eV) as the temperature increases from 77 to 700 K.

III. RESULTS

Our first objective is to determine the bandgap E_0 as a function of temperature. To achieve this, one typically plots the square of the absorption coefficient as a function of photon energy (Tauc plot) and then finds the bandgap by extrapolating to zero.[5] We could only find a linear region in such Tauc plots below room temperature and, therefore, chose not to use this method.

Instead, we described the pseudodielectric function of InSb with the Herzinger–Johs parametric semiconductor model[53] and varied the parameters of the direct bandgap as a function of temperature until a good fit was achieved. This model has been shown to work well for the direct gap of Ge over a broad range of temperatures.[52] In particular, the direct bandgaps of Ge determined from the parametric semiconductor model agreed well with those obtained using second-derivative and reciprocal space methods, see Fig. 6 in Ref. 52.

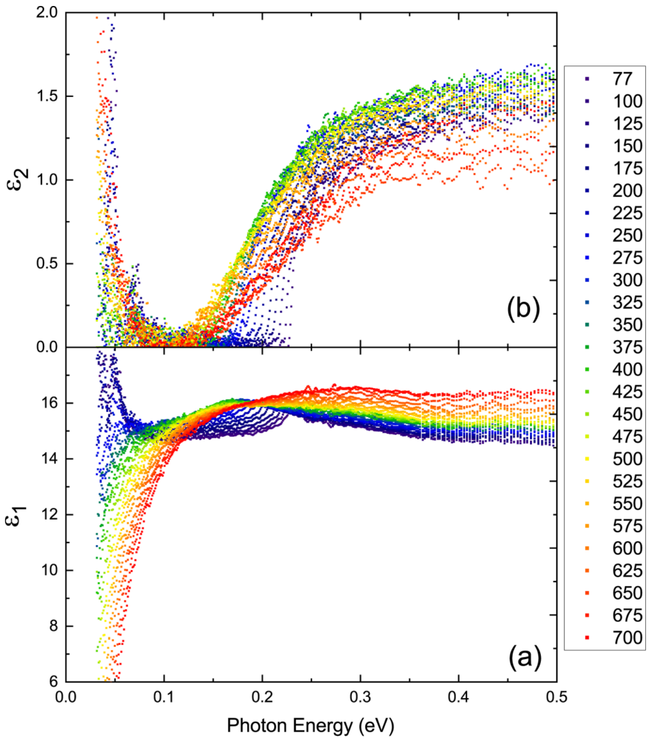

FIG. 1. Real (a) and imaginary (b) parts of the dielectric function of InSb (100) at temperatures from 77 to 700 K in steps of 25 K, after correction for an oxide thickness of 25 Å.

At elevated temperatures, a Drude term[5]

$$\Delta\epsilon_{\mathrm{Drude}}(\omega) = -\frac{\omega_P^2}{\omega^2 + i\gamma\omega} = -\frac{ne^2}{m^* m_0 \epsilon_0(\omega^2 + i\gamma\omega)} \qquad (1)$$

was added to the parametric semiconductor dielectric function to describe absorption by free electrons, where $\hbar\omega$ is the photon energy, ω_P is the (angular) plasma frequency, n is the free electron density, e is the electronic charge, $m^* m_0$ is the effective electron mass ($m^* = 0.014$, which we kept independent of temperature), ϵ_0 is the permittivity of vacuum, and γ is the electron scattering rate. (The absorption by free holes was neglected due to their large effective mass.) The mobility can be calculated from Ref. 54, $\mu = e/\gamma m_0 m^*$.

Examples of such fits are shown in Fig. 2. The agreement between data and fit is usually quite good. It may be possible to achieve an even better agreement with the lineshapes for screened excitons proposed by Tanguy,[39,41] which will be discussed in more detail below. We recently applied the excitonic (Tanguy) line shapes to the direct bandgap of Ge, with good success.[55] In particular, the broadenings for InSb may be somewhat smaller than those obtained from a parametric semiconductor fit. The asymmetry of the experimental line shape leads to a slight over-estimation of the bandgap values by a few meV.

Published under an exclusive license by the AVS

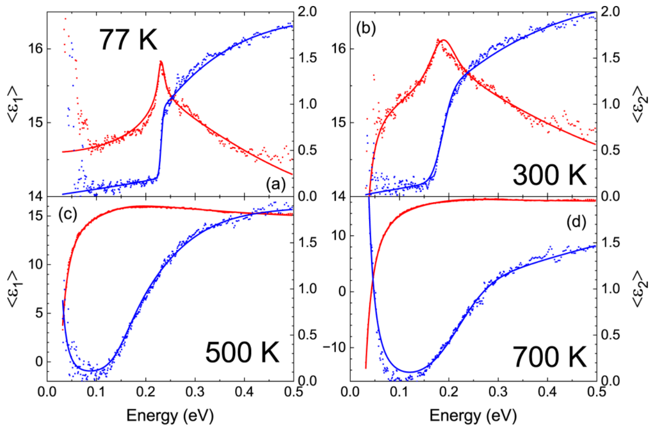

FIG. 2. Real (red) and imaginary (blue) parts of the pseudodielectric function of InSb (100) at temperatures from 77 to 700 K (abcd, symbols) in comparison to the parametric semiconductor model with a Drude term, see Eq. (1) (solid).

The direct bandgaps and broadenings of InSb as a function of temperature obtained from the parametric semiconductor fit are shown in Fig. 3. As already observed by inspection of the dielectric functions in Fig. 1, the bandgap decreases up to 450 K, remains approximately constant up to 600 K, and then increases again at the highest temperatures by about 50–70 meV. Figure 3 also shows the broadening parameter of the direct bandgap, which increases more or less monotonically with temperature. The broadenings of E_0 in InSb are at least five times larger than in Ge[55] but comparable to GaP[56] and GaAs.[57] The last data point at 725 K is very close to the melting point of our sample.

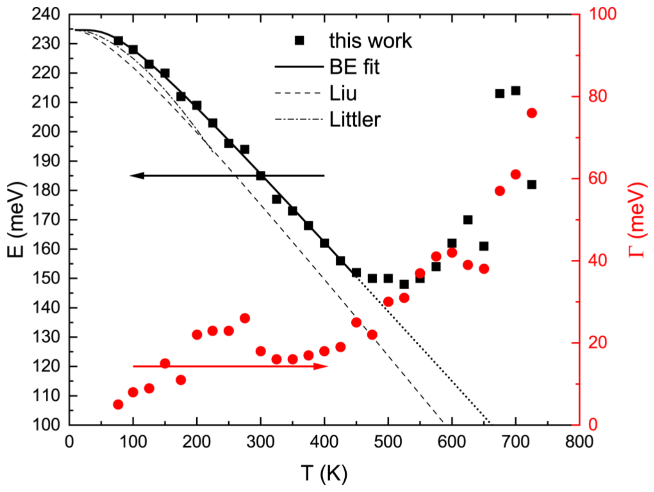

FIG. 3. Direct bandgap E_0 (■) and broadening Γ (•) of InSb as a function of temperature. The solid line shows the best fit to Eq. (2) up to 450 K. It is extrapolated at elevated temperatures by the dotted line. Results from the literature (Refs. 28 and 37) are also shown.

TABLE I. Bose–Einstein parameters for the temperature dependence of the direct bandgap E_0 expressed in Eq. (2).

E_B (meV)	a_B (meV)	Ω (meV)	Source
261 ± 4	26 ± 6	14 ± 2	This work
260	24	15	Ref. 9 (theory)

Our bandgaps agree reasonably well with prior results[28,37] at low temperatures. There are some differences at higher temperatures that could be explained by errors in the temperature measurement on the order of 50 K, which is not uncommon at such high temperatures.

Up to 450 K, the dependence of the bandgap can be described with a Bose–Einstein model,[29,45]

$$E(T) = E_B - a_B\left[1 + \frac{2}{\exp(\Omega/k_B T) - 1}\right], \tag{2}$$

where E_B is the unrenormalized bandgap (in the absence of electron-phonon interactions), T is the temperature, a_B is the strength of the electron-phonon interaction, Ω is an effective phonon energy, and k_B is the Boltzmann constant. Parameters obtained from our experimental data are shown in Table I and are in good agreement with the literature.[9]

By fitting the data shown in Fig. 1 with Eq. (1), we were also able to determine the carrier concentration n and the mobility μ, which are shown in Fig. 4. Strictly speaking, Eq. (1) yields a plasma frequency and a scattering rate. This can be converted into a carrier density and mobility, if the effective mass m^* is known. Through

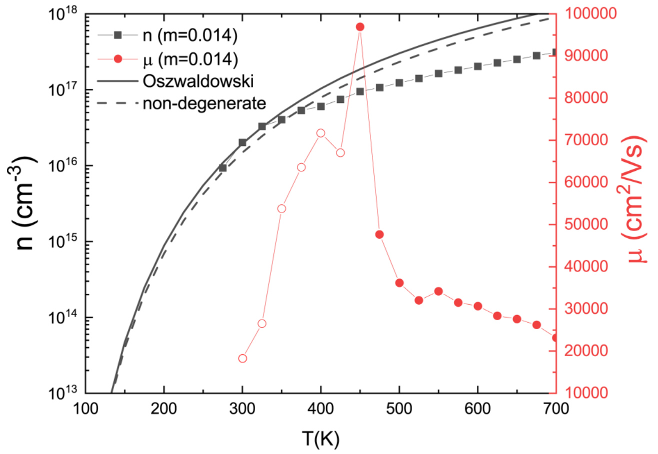

FIG. 4. Carrier concentration n (■) and mobility μ (•) determined using a Drude fit to the dielectric functions shown in Fig. 1 assuming a temperature-independent effective electron mass of $m^* = 0.014$. The errors for μ are large below 450 K, indicated by open symbols. The carrier concentration in the nondegenerate limit (dashed) (Refs. 21 and 22), with the bandgap taken from Eq. (2) and $m^* = 0.014$, and from Ref. 15 (solid) are also shown.

Published under an exclusive license by the AVS

$\vec{k}\cdot\vec{p}$-theory, m^* depends on the bandgap. One should also include the carrier-density dependence of m^* due to the large nonparabolicity of the conduction band.[42] Such considerations are beyond the scope of the present article and we keep the effective mass constant at $m^* = 0.014$ for free electrons in InSb. The Drude contributions of holes are much smaller (due to the large mass of heavy holes and the low concentration of light holes) and have been neglected.

At low temperatures, the Drude response of free carriers is masked by depolarization effects (backside reflections), but at 275 K and above, there is a clear decrease in ϵ_1 at low energies, see Fig. 2, which yields the plasma frequency and electron concentration. The increase in ϵ_2 at low energies is damped by a factor of γ/ω compared to ϵ_1, see Eq. (1), and only visible at 450 K and higher, see Fig. 4. The carrier density n derived from our plasma frequency data with $m^* = 0.014$ agrees well with a simple nondegenerate model (dashed) and an analysis of temperature-dependent Hall effect measurements (solid) near room temperature, see Fig. 4. At higher temperatures, we underestimate the electron concentration because of our assumption of a constant electron mass. If we correctly calculated the temperature-dependent mass, our electron concentration would likely be closer to the literature results.

Below 450 K, the scattering rate and mobility parameters in the Drude fit have very large error bars (as indicated by open symbols in Fig. 4) and should be ignored. Between 450 and 700 K, the mobility decreases from 100 000 to 20 000 $\mathrm{cm}^2/\mathrm{Vs}$, consistent with Hall effect measurements.[58]

IV. DISCUSSION, SUMMARY, AND OUTLOOK

In summary, we determined the infrared dielectric function of InSb in the region of the direct bandgap at temperatures from 77 to 725 K using Fourier-transform infrared spectroscopic ellipsometry. The native oxide thickness was determined to be 25 ± 5 Å using the Jellison–Sales method for transparent glasses and appropriate corrections were made to the experimental data.

We observe a decrease in the direct bandgap up to 450 K due to electron-phonon interactions and thermal expansion, which can be described with a Bose–Einstein model, similar to direct bandgaps in other semiconductors. The broadening increases with temperature. At the lowest photon energies (below 0.1 eV), there is a Drude tail, from which the free electron concentration and the electron mobility can be determined. We underestimate the electron concentration and overestimate the Fermi energy and the mobility because we assumed a constant effective mass and ignored the conduction band nonparabolicity in our analysis, see Fig. 1 in Ref. 6, but this does not change our conclusions qualitatively.

At the highest temperatures, the free carrier concentration due to thermally excited electron-hole pairs becomes very large and the Fermi level is above the conduction band minimum.[6] This reduces the magnitude of ϵ_2 due to band filling and screening of the excitonic (Sommerfeld) enhancement of absorption. Band filling also results in a thermal Burstein–Moss shift: The onset of absorption is larger than the bandgap by about 100 meV at 700 K due to band filling. Therefore, the observed bandgap increases again above 600 K.

A more complete model would attempt to describe ϵ_2 of InSb with the absorption of screened excitons given by Tanguy,[38,39,41]

$$\epsilon_2(\hbar\omega) = \frac{2\pi A\sqrt{R}}{(\hbar\omega)^2} \times \left\{ \sum_{n=1}^{\sqrt{g}} \frac{2R}{n}\left(\frac{1}{n^2} - \frac{n^2}{g^2}\right)\delta\left[\hbar\omega - E_0 + \frac{R}{n^2}\left(1 - \frac{n^2}{g}\right)^2\right] + \frac{\sinh(\pi g k) H(\hbar\omega - E_0)}{\cosh(\pi g k) - \cosh\left(\pi g\sqrt{k^2 - \frac{4}{g}}\right)} \right\} [f_h(\hbar\omega) - f_e(\hbar\omega)]. \tag{3}$$

A and R are the excitonic amplitude and binding energy, respectively, for transitions from the heavy hole to the electron band. (Transitions from the light hole and split-off hole bands could be added, but they are smaller.) The parameters A and R need to be corrected for nonparabolicity effects. Another correction may be needed to take into account the k-dependence of the momentum matrix element.[25] E_0 is the bandgap, i.e., the energy difference between the conduction band minimum and the valence band maximum. E_0 depends on temperature and on the carrier concentration due to many-body effects (band bap renormalization).[59,60] The first term in brackets describes the absorption of the nth discrete exciton, and the second term describes the absorption by the exciton continuum. g is the Hulthen potential screening parameter,[40] which can be calculated from the Thomas–Fermi screening length. H is the Heaviside unit step function and $k = \sqrt{(\hbar\omega - E_0)/R}$. The functions f_h and f_e describe band filling and are calculated from the degenerate Fermi–Dirac distribution functions in the valence and conduction bands.[38] The real part can be found by Kramers–Kronig transformation, after introducing Lorentzian broadenings of transitions.[41] Modifications are also required to take into account the effects of nonparabolicity on free carrier absorption.

A numerical evaluation of this expression is beyond the scope of the present article and will be presented elsewhere.

ACKNOWLEDGMENTS

This work was supported by the Air Force Office of Scientific Research (AFOSR) under Award No. FA9550-20-1-0135. J.R.L. and C.M.Z. acknowledge support from the New Mexico Alliance for Minority Participation (NMAMP).

AUTHOR DECLARATIONS

Conflict of Interest

The authors have no conflicts to disclose.

Author Contributions

Melissa Rivero Arias: Data curation (lead); Formal analysis (lead); Investigation (lead); Visualization (lead); Writing – review & editing (supporting). **Carlos A. Armenta:** Data curation (supporting); Formal analysis (supporting); Investigation (supporting);

Published under an exclusive license by the AVS

Supervision (equal); Validation (supporting). **Carola Emminger:** Data curation (supporting); Formal analysis (equal); Investigation (supporting); Software (lead); Supervision (equal); Validation (equal); Writing – review & editing (supporting). **Cesy M. Zamarripa:** Data curation (equal); Formal analysis (supporting); Investigation (equal); Visualization (equal). **Nuwanjula S. Samarasingha:** Supervision (equal); Validation (equal). **Jaden R. Love:** Investigation (supporting); Resources (equal). **Sonam Yadav:** Formal analysis (lead). **Stefan Zollner:** Conceptualization (lead); Data curation (supporting); Formal analysis (supporting); Funding acquisition (lead); Project administration (lead); Resources (lead); Supervision (lead); Validation (lead); Visualization (supporting); Writing – original draft (lead); Writing – review & editing (lead).

DATA AVAILABILITY

The data that support the findings of this study are available from the corresponding author upon reasonable request.

REFERENCES

[1] P. Y. Yu and M. Cardona, *Fundamentals of Semiconductors* (Springer, Berlin, 2010).

[2] H. C. Casey and M. B. Panish, *Heterostructure Lasers* (Academic, New York, 1978), Part B.

[3] C. Hilsum and A. C. Rose-Innes, *Semiconducting III-V Compounds* (Pergamon, Oxford, 1961).

[4] P. Lawaetz, Phys. Rev. B **4**, 3460 (1971).

[5] M. Fox, *Optical Properties of Solids* (Oxford University, Oxford, 2010).

[6] R. A. Masut, Eur. J. Phys. **43**, 015501 (2022).

[7] D. J. Lockwood, G. Yu, and N. L. Rowell, Solid State Commun. **136**, 404 (2005).

[8] J. R. Chelikowsky and M. L. Cohen, Phys. Rev. B **14**, 556 (1976); **30**, 4828 (E) (1984).

[9] N. Bouarissa and H. Aourag, Infrared Phys. Technol. **38**, 153 (1997).

[10] W. Shockley, *Electrons and Holes in Semiconductors* (Van Nostrand, Princeton, 1950), p. 242.

[11] H. J. Hrostowski, F. J. Morin, T. H. Geballe, and G. H. Wheatley, Phys. Rev. **100**, 1672 (1955).

[12] R. W. Cunningham and J. B. Gruber, J. Appl. Phys. **41**, 1804 (1970).

[13] P. W. Kruse, Semicond. Semimetals **5**, 15 (1970).

[14] V. V. Kosarev, V. V. Popov, V. S. Vekshina, and N. I. Pepik, Phys. Status Solidi A **107**, K43 (1988).

[15] M. Oszwaldowski and M. Zimpel, J. Phys. Chem. Solids **49**, 1179 (1988).

[16] E. O. Kane, J. Phys. Chem. Solids **1**, 82 (1956).

[17] E. Burstein, Phys. Rev. **93**, 632 (1954).

[18] T. S. Moss, Proc. Phys. Soc. B **67**, 775 (1954).

[19] P. K. Chakraborty, G. C. Datta, and K. P. Ghatak, Physica B **339**, 198 (2003).

[20] J. S. Blakemore, J. Appl. Phys. **53**, 520 (1982).

[21] N. W. Ashcroft and N. D. Mermin, *Solid State Physics* (Saunders, Philadelphia, 1976).

[22] S. M. Sze, *Physics of Semiconductor Devices* (Wiley, New York, 1981).

[23] T. S. Moss, S. D. Smith, and T. D. F. Hawkins, Proc. Phys. Soc. B **70**, 776 (1957).

[24] G. W. Gobeli and H. Y. Fan, Phys. Rev. **119**, 613 (1960).

[25] E. J. Johnson, *Semiconductors and Semimetals* (Academic, New York, 1967), Vol. 3, pp. 153–258.

[26] S. T. Schaefer, S. Gao, P. T. Webster, R. R. Kosireddy, and S. R. Johnson, J. Appl. Phys. **127**, 165705 (2020).

[27] S. W. Kurnick and J. M. Powell, Phys. Rev. **116**, 597 (1959).

[28] P. Y. Liu and J. C. Maan, Phys. Rev. B **47**, 16274 (1993);*ibid.* **47**, 16279 (1993).

[29] S. Logothetidis, L. Viña, and M. Cardona, Phys. Rev. B **31**, 947 (1985).

[30] T. J. Kim, S. Y. Hwang, J. S. Byun, M. S. Diware, J. Choi, H. G. Park, and Y. D. Kim, J. Appl. Phys. **114**, 103501 (2013).

[31] S. Zollner, S. Gopalan, and M. Cardona, Solid State Commun. **77**, 485 (1991).

[32] C. Larez and C. Rincon, Mat. Lett. **24**, 211 (1995).

[33] V. Roberts and J. E. Quarrington, J. Electron. Control **1**, 152 (1955).

[34] N. L. Rowell, Infrared Phys. **28**, 37 (1988).

[35] Z. M. Fang, K. Y. Ma, D. H. Jaw, R. M. Cohen, and G. B. Stringfellow, J. Appl. Phys. **67**, 7034 (1990).

[36] D. Auvergne, J. Camassel, H. Mathieu, and M. Cardona, Phys. Rev. B **9**, 5168 (1974).

[37] C. L. Littler and D. G. Seiler, Appl. Phys. Lett. **46**, 986 (1985).

[38] J. Menéndez, C. Poweleit, and S. E. Tilton, Phys. Rev. B **101**, 195204 (2020).

[39] C. Tanguy, Phys. Rev. Lett. **75**, 4090 (1995);*ibid.* **76**, 716 (1996) (E).

[40] L. Bányai and S. W. Koch, Z. Phys. B **63**, 283 (1986).

[41] C. Tanguy, Phys. Rev. B **60**, 10660 (1999).

[42] W. Zawadzki, Adv. Phys. **23**, 435 (1974).

[43] Y. J. Jung, M. K. Park, S. I. Tae, K. H. Lee, and H. J. Lee, J. Appl. Phys. **69**, 3109 (1991).

[44] E. S. Koteles and W. R. Datars, Phys. Rev. B **9**, 568 (1974).

[45] S. Zollner, F. Abadizaman, C. Emminger, and N. Samarasingha, Adv. Opt. Technol. **11**, 117 (2022).

[46] L. I. Berger, *Semiconductor Materials* (CRC, Boca Raton, 1997).

[47] D. E. Aspnes and A. A. Studna, Phys. Rev. B **27**, 985 (1983).

[48] H. J. Mattausch and D. E. Aspnes, Phys. Rev. B **23**, 1896 (1981).

[49] S. Zollner, Appl. Phys. Lett. **63**, 2523 (1993).

[50] G. E. Jellison and B. C. Sales, Appl. Opt. **30**, 4310 (1991).

[51] N. S. Samarasingha and S. Zollner, J. Vac. Sci. Technol. B **39**, 052201 (2021).

[52] C. Emminger, F. Abadizaman, N. S. Samarasingha, T. E. Tiwald, and S. Zollner, J. Vac. Sci. Technol. B **38**, 012202 (2020).

[53] C. M. Herzinger and B. Johs, U.S. patent 5,796,983 (18 August 1998).

[54] S. Zollner, P. P. Paradis, F. Abadizaman, and N. S. Samarasingha, J. Vac. Sci. Technol. B **37**, 012904 (2019).

[55] C. Emminger, N. S. Samarasingha, M. Rivero Arias, F. Abadizaman, J. Menendez, and S. Zollner, J. Appl. Phys. **131**, 165701 (2022).

[56] S. Zollner, M. Garriga, J. Kircher, J. Humlíček, M. Cardona, and G. Neuhold, Phys. Rev. B **40**, 7915 (1993).

[57] P. Lautenschlager, M. Garriga, S. Logothetidis, and M. Cardona, Phys. Rev. B **35**, 9174 (1987).

[58] D. L. Rode, Phys. Rev. B **3**, 3287 (1971).

[59] V. Vashista and R. K. Kalia, Phys. Rev. B **25**, 6492 (1982).

[60] R. Zimmerman, Phys. Status Solidi B **146**, 371 (1988).

[61] See supplementary material at https://www.scitation.org/doi/suppl/10.1116/6.0002326 for additional experimental data and figures and for a simple model calculation of the Burstein–Moss shift.

Published under an exclusive license by the AVS

Supplementary Material for "Temperature dependence of the infrared dielectric function and the direct band gap of InSb from 80 to 725 K"

(Dated: 12 January 2023)

Melissa Rivero Arias, Carlos A. Armenta, Carola Emminger, Cesy M. Zamarripa, Nuwanjula S. Samarasingha, Jaden R. Love, Sonam Yadav, and Stefan Zollner

Department of Physics, MSC 3D, New Mexico State University, P. O. Box 30001, Las Cruces, NM 88003-8001, USA

S1. PSEUDODIELECTRIC FUNCTIONS

The pseudodielectric functions of undoped InSb (100) at room temperature in air before and after the wet clean described in the main text are shown in Fig. S1. Using the data of Aspnes and Studna[47] as the reference for the optical constants of bare InSb (augmented by unpublished data from the University of Nebraska below 1.5 eV and above 6.0 eV provided by the J. A. Woollam Company) and those of Refs. 48 and 49 for its native oxide, we find oxide thicknesses of 36 Å (before wet cleaning) and 29 Å (after wet cleaning). To obtain these oxide thicknesses, we compare the maximum of $<\epsilon_2>$ at the E_2 critical point near 3.7 eV. Our E_2 maximum is redshifted by about 0.1 eV compared to Ref. 47. We verified the wavelength calibration of our HS-190 monochromator with a bare Si wafer and do not believe that there is an issue with our equipment. This wavelength calibration error does not matter for the optical constants near the direct band gap reported here, since they were determined using a different instrument.

Figure S2 shows the pseudodielectric functions of InSb (100) at 300 K in air after a water/isopropanol wet clean from 0.03 to 6.5 eV, taken on both FTIR-VASE (blue) and VASE (green) instruments, in comparison to a point-by-point fit to the merged data set for the dielectric function, assuming an oxide thickness of 29 Å (red). The data are merged well in the region of overlap, but the noise of the FTIR-VASE data is large above 0.7 eV. The direct band gap E_0 can clearly be seen by the onset of absorption in $\langle\epsilon_2\rangle$ and with a peak in $\langle\epsilon_1\rangle$ at about 0.2 eV.

The native oxide thickness of the InSb sample at 300 K in UHV (after heating the sample overnight) was found to be 25±5 Å using the Jellison-Sales method for transparent glasses,[50] which is explained in the main text and in Fig. S3. This is somewhat lower than in air (29 Å), as expected.

The pseudodielectric function of InSb (100) at temperatures from 77 K to 700 K in steps of 25 K is shown in Fig. S4. These data are corrected for window effects by the software of the instrument manufacturer, but not for oxide overlayers.

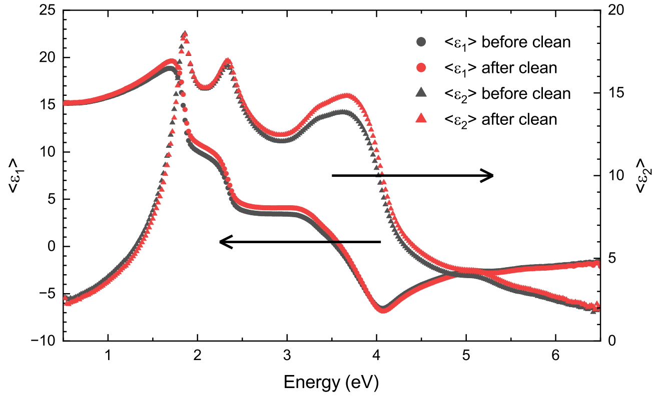

FIG. S1. Real (●) and imaginary (▲) parts of the pseudodielectric function of InSb (100) at 300 K in air before (black) and after (red) a water/isopropanol wet clean resulting in native oxide thicknesses of 36 and 29 Å before and after the clean, respectively.

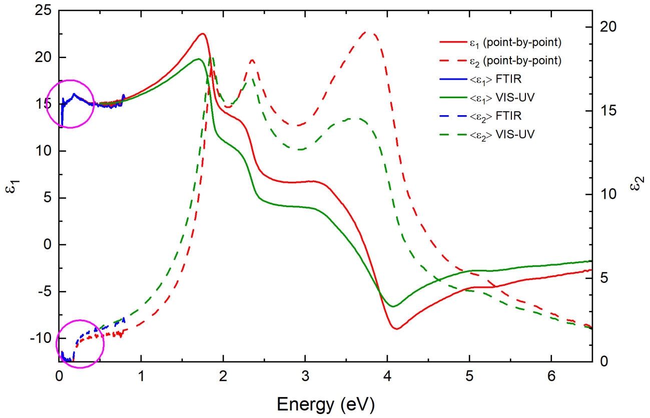

FIG. S2. Real (solid) and imaginary (dashed) parts of the pseudodielectric functions of InSb (100) at 300 K in air after a water/isopropanol clean from 0.03 to 6.5 eV, taken on both FTIR-VASE (blue) and VASE (green) instruments. Both data sets are merged well in the region of overlap (0.5 to 0.7 eV). The red lines show the results of a point-by-point fit to the merged data set for the dielectric function with an oxide correction of 29 Å. The magenta circles show the region of the direct band gap E_0.

A few things are noteworthy as a qualitative interpretation of the pseudodielectric function: (1) $<\epsilon_2>$ is slightly positive in the range from 0.1 to 0.2 eV (below the band gap) due to the effects of the native oxide, requiring a correction to determine the dielectric function ϵ_2. (2) The E_0 band gap, seen as the onset of absorption and as a peak of $<\epsilon_1>$, decreases from the lowest temperatures (purple) to room temperature (blue), then remains constant to 500 K (yellow), and then increases again at the highest temperatures (red). (3) The broadening increases monotonically with temperature. (4) Above room

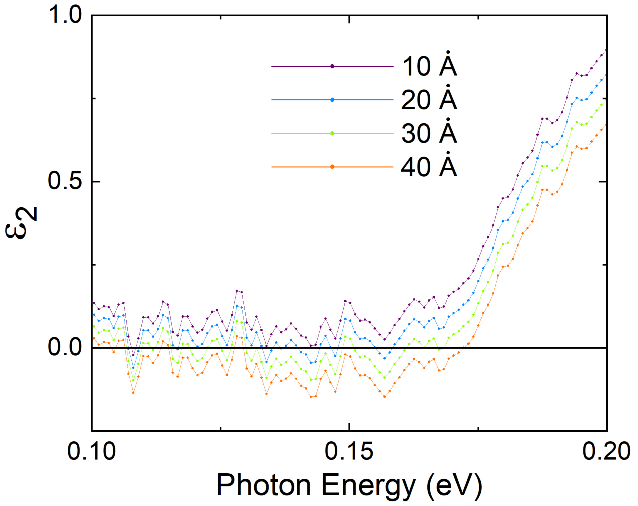

FIG. S3. Imaginary part of the corrected dielectric function in the transparent region of undoped InSb below the band gap at 300 K in UHV, for different assumed oxide thicknesses. For 40 Å oxide thickness, ϵ_2 is negative and the data was overcorrected. For 10 Å oxide thickness, ϵ_2 is positive and the data was undercorrected. This results in our estimate of 25±5 Å for the native oxide thickness in this measurement.

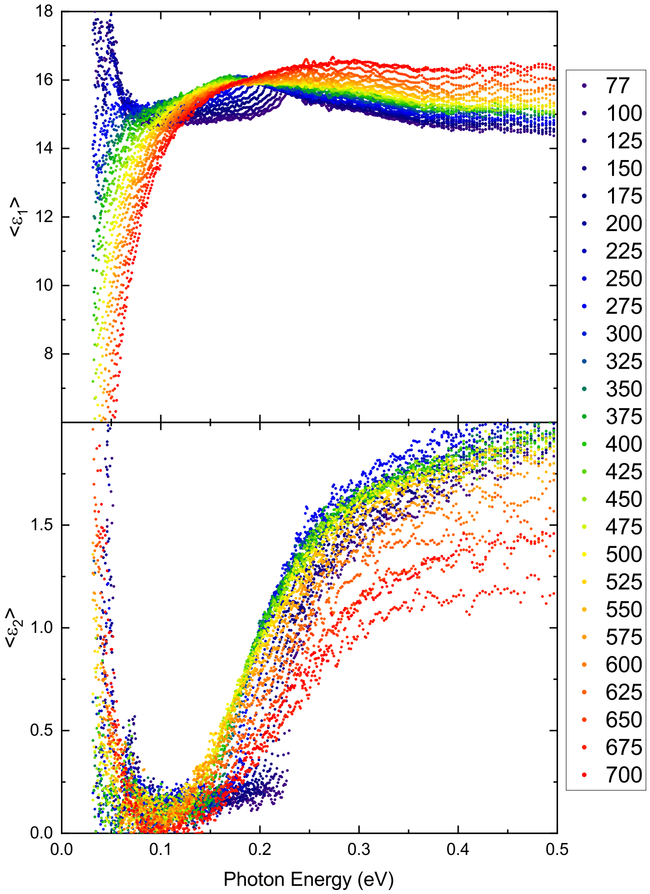

FIG. S4. Real (a) and imaginary (b) parts of the pseudodielectric function of InSb (100) at temperatures from 77 K to 700 K in steps of 25 K.

temperature, $<\epsilon_1>$ diverges towards $-\infty$ at the lowest photon energies, while $<\epsilon_2>$ diverges towards $+\infty$. This indicates free carrier absorption, described with a Drude model, at elevated temperatures. (5) There is a decrease of $<\epsilon_2>$ at the highest temperatures due to band filling.

S2. DEGENERATE CARRIER STATISTICS FOR INSB

For an undoped (intrinsic) semiconductor with parabolic bands, the electron and hole concentrations as a function of temperature T are given by[38]

$$n\left(T\right) = \frac{1}{4}\left(\frac{2m_0 m_e k_B T}{\pi\hbar^2}\right)^{\frac{3}{2}} F_{\frac{1}{2}}\left(\frac{\mu - E_0}{k_B T}\right) \quad \text{(S1)}$$

$$p\left(T\right) = \frac{1}{4}\left(\frac{2m_0 m_h k_B T}{\pi\hbar^2}\right)^{\frac{3}{2}} F_{\frac{1}{2}}\left(\frac{-\mu}{k_B T}\right), \quad \text{(S2)}$$

respectively, where m_e and m_h are the effective density-of-states masses of the conduction and valence bands and $\hbar$ is the reduced Planck's constant. μ is the chemical potential, and E_0=0.2 eV is the direct band gap, which we have assumed to be constant, ignoring the reduction of the band gap due to thermal expansion and electron-phonon scattering. We also assumed constant effective masses. All energies are measured relative to the top of the valence band. (See also: J.S. Blakemore, *Semiconductor Statistics*, Pergamon, Oxford, 1962, Eq. 240.1)

For sufficiently low temperatures, the argument of the Fermi-Dirac integral $F_{\frac{1}{2}}$ becomes very large and the Fermi integral can be expanded into (J. McDougall and E.C. Stoner, *The computation of Fermi-Dirac functions*, Philos. Trans. R. Soc. London **237**, 67-104, 1938; J.S. Blakemore, *Approximations for Fermi-Dirac integrals, especially the function $F_{\frac{1}{2}}\left(\eta\right)$ used to describe electron density in a semiconductor*, Solid-State Electron. **25**, 1067-1076, 1982)

$$F_{\frac{1}{2}}\left(\eta\right) \approx \frac{4\eta^{\frac{3}{2}}}{3\sqrt{\pi}} \quad \text{for large } \eta, \quad \text{(S3)}$$

essentially using Maxwell-Boltzman statistics to describe the electron and hole populations. This approximation leads to the well-known expressions[21,22]

$$\mu \approx \frac{E_0}{2} + \frac{3k_B T}{4}\ln\left(\frac{m_h}{m_e}\right) \quad \text{and} \quad \text{(S4)}$$

$$n \approx 2\left(\frac{m_0 k_B T}{2\pi\hbar^2}\right)^{\frac{3}{2}} \left(m_e m_h\right)^{\frac{3}{4}} \exp\left(-\frac{E_0}{2k_B T}\right). \quad \text{(S5)}$$

For InSb, these expressions can be used up to 300 K, but deviations become noticeable at higher temperatures. Above 300 K, we must use the exact definition of the Fermi-Dirac integral (Blakemore, 1982; Blakemore, 1962,

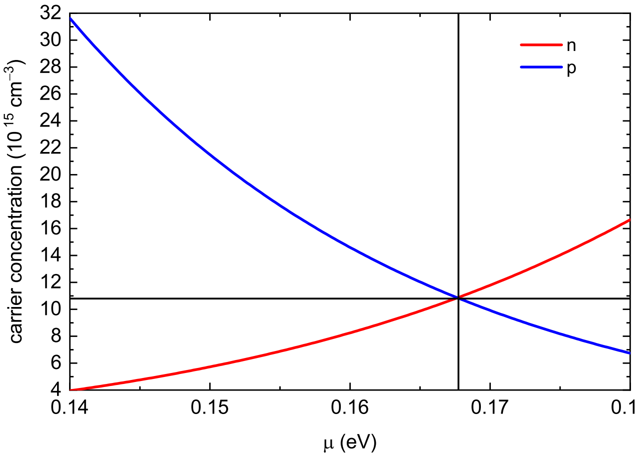

FIG. S5. Electron and hole concentrations n and p of InSb calculated with Eqs. (S1) and (S2) as a function of chemical potential μ at 300 K. This calculation assumes parabolic bands and a constant band gap of 0.2 eV and constant effectives masses. The two curves cross at the intrinsic chemical potential of 168 meV.

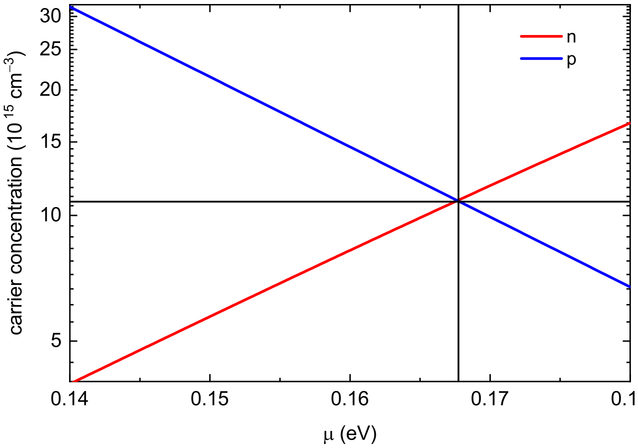

FIG. S6. As Fig. S5, but on a logarithmic scale. Compare Fig. 16.2 in Ref. 10.

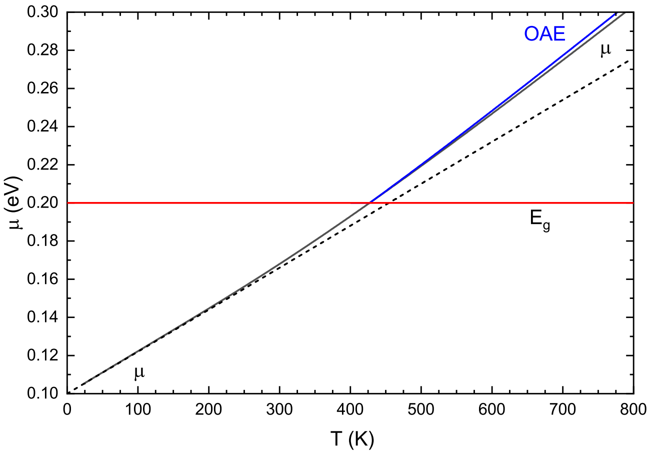

FIG. S7. Chemical potential for intrinsic InSb versus temperature in the degenerate (solid) and non-degenerate (dotted) case. The red horizontal line shows the band gap of 0.2 eV. The blue line shows the optical activation energy (OAE, i.e., the experimental band gap) given by Eq. (S8). This calculation assumes parabolic bands, a constant band gap, and constant effective masses. Compare Fig. 2 in Ref. 15.

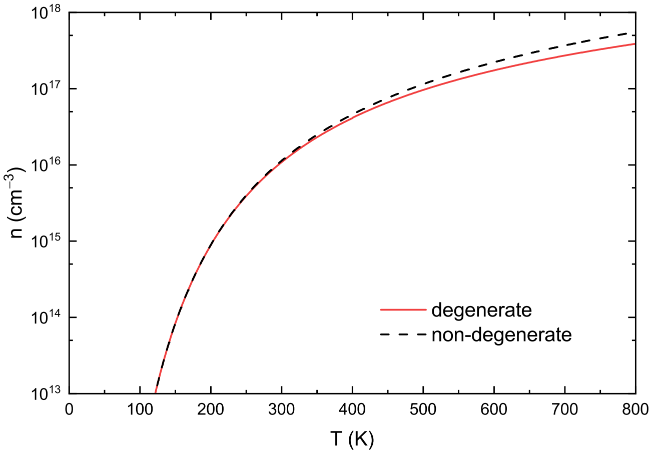

FIG. S8. Electron and hole concentrations as a function of temperature calculated using Eqs. (S1) and (S2) from the degenerate chemical potential shown in Fig. S7 (solid). The non-degenerate carrier concentration from Eq. (S5) is also shown (dashed). This calculation assumes parabolic bands, a constant band gap, and constant effective masses. Compare Fig. 1 in Ref. 15.

Eq. 210.3)

$$F_{\frac{1}{2}}\left(\eta\right)=\frac{2}{\sqrt{\pi}}\int_{0}^{\infty}\frac{\sqrt{y}}{\exp\left(y-\eta\right)+1}dy. \tag{S6}$$

We evaluate the Fermi-Dirac integrals $F_{\frac{1}{2}}$ by noting their connection (M.D. Ulrich, W.F. Seng, and P.A. Barnes, *Solutions to the Fermi-Dirac integrals in semiconductor physics using polylogarithms*, J. Comp. Electronics **1**, 431, 2002)

$$F_n\left(\eta\right)=-Li_{n+1}\left(-e^{\eta}\right) \tag{S7}$$

with polylogarithm functions Li_{n+1}, which were calculated using the `polylog()` function in MATLAB.

In an intrinsic semiconductor, electrical neutrality requires that $n\left(T\right)$=$p\left(T\right)$ (Blakemore, 1962, Sec. 2.3). For a given temperature T, we therefore plot n and p as a function of μ. The intrinsic chemical potential is found at the location where the two lines cross. As an example, we show the electron and hole concentrations as a function of the chemical potential at 300 K in Figs. S5 and S6. The two curves cross at the intrinsic chemical potential of 168 meV at 300 K.

We then vary the temperature from 25 to 800 K and calculate the intrinsic chemical potential at each step. See Fig. S7 for results. Below 25 K, the dependence of the carrier concentration on the chemical potential is very

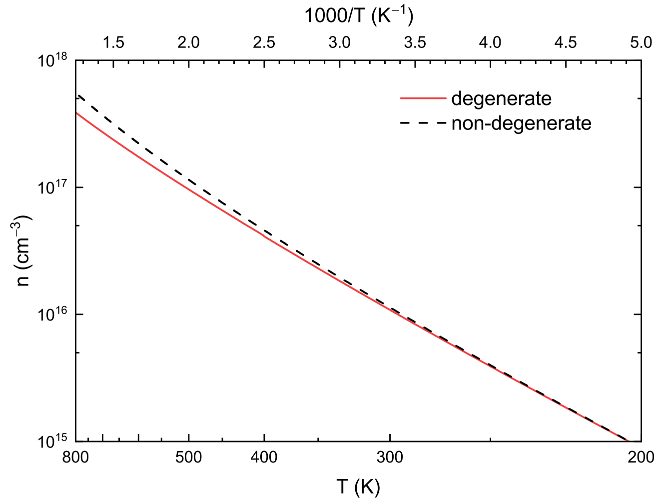

FIG. S9. As Fig. S8, but with an Arrhenius (inverse reciprocal temperature) scale. Compare Ref. 11 and Fig. 23.6 in Blakemore, 1962.

weak and we therefore use Eq. (S4) in the non-degenerate limit to calculate the chemical potential below 25 K. As expected from Eq. (S4), the chemical potential increases linearly with temperature in the non-degenerate limit (dashed). The degenerate chemical potential (solid) increases superlinearly with temperature and is somewhat larger than for the non-degenerate limit. The two curves start to separate bove 200 K. Near 400 K, the chemical potential is equal to the band gap. This means that the Fermi level crosses over into the conduction band, making InSb fully degenerate.

Once the chemical potential μ is known, the electron and hole concentration can be calculated from Eqs. (S1) or (S2), see Figs. S8 and S9. At high temperatures, the carrier concentration is somewhat lower in the degenerate case (solid) than in the classical non-degenerate (Maxwell-Boltzmann) limit, see also Fig. 23.8 in Blakemore (1962). Since the $T^{3/2}$ dependence is much weaker than the exponential dependence on temperature in Eq. (S5), the carrier concentration varies nearly linearly when drawn with a reverse inverse temperature (Arrhenius) scale, see Fig. S9. At 700 K, the carrier concentration calculated from this simple model is in the mid-10^{17} cm^{-3} range, of the same order of magnitude as the experimental data shown in Fig. 4.

The optical activation energy (OAE, i.e., the experimental band gap measured with transmission or ellipsometry measurements) is given by[19]

$$E_A = \max\left[E_0, E_0 + \left(1 + \frac{m_e}{m_h}\right)(\mu - E_0)\right]. \qquad \text{(S8)}$$

Due to the small electron to hole mass ratio, the OAE is almost the same as the chemical potential, once μ is larger than the band gap (above about 400 K). The OAE is also shown in Fig. S7. It is apparent that there is a thermal Burstein-Moss shift for temperatures above 400 K, because the chemical potential and the OAE are larger than the intrinsic band gap. This Burstein-Moss shift is about 0.1 eV at 750 K, which is similar to the difference between the experimental band gap (■) and the dotted line in Fig. 3.

Additional calculations will be carried out to take into account the temperature dependence of the band gap and the effective masses as well as the non-parabolicity of the conduction band.